Article:
Cheng, H., Pan, S. and Di Valentino, E. (2026) Beyond two parameters: revisiting dark energy with the latest cosmic probes. The Astrophysical Journal, 999 (2). 190. ISSN: 0004-637X

https://doi.org/10.3847/1538-4357/ae3a8f

The Astrophysical Journal, 999:190 (14pp), 2026 March 10 https://doi.org/10.3847/1538-4357/ae3a8f

Beyond Two Parameters: Revisiting Dark Energy with the Latest Cosmic Probes

Hanyu Cheng[1,2,3], Supriya Pan[4,5], and Eleonora Di Valentino[3]
[1] Tsung-Dao Lee Institute (TDLI), No. 1 Lisuo Road, 201210 Shanghai, People's Republic of China; hcheng19@sheffield.ac.uk
[2] School of Physics and Astronomy, Shanghai Jiao Tong University, 800 Dongchuan Road, 200240 Shanghai, People's Republic of China
[3] School of Mathematical and Physical Sciences, University of Sheffield, Hounsfield Road, Sheffield S3 7RH, UK; e.divalentino@sheffield.ac.uk
[4] Department of Mathematics, Presidency University, 86/1 College Street, Kolkata 700073, India; supriya.maths@presiuniv.ac.in
[5] Institute of Systems Science, Durban University of Technology, Durban 4000, South Africa
Received 2025 October 20; revised 2025 December 17; accepted 2026 January 15; published 2026 March 3

Abstract

Dark energy (DE) models with many free parameters are often considered excessive, as constraining all parameters poses a significant challenge. While such models offer greater flexibility to probe the DE sector in more detail. With the rapid advancement of astronomical surveys and the availability of diverse datasets, it is timely to examine whether current combined observations can effectively constrain an extended parameter space in DE models. This article investigates a four-parameter dynamical DE model that spans a broad region of the Universe's expansion history through four key parameters: present-day value of the DE equation of state (w_0), its initial value (w_m), scale factor depicting transition from w_m to w_0 (a_t), and steepness of this transition ($\Delta_{\rm de}$). We constrain the model using cosmic microwave background data from Planck, BAO from DESI DR2, and three distinct compilations of Type Ia Supernovae: PantheonPlus, DESY5, and Union3. Our results show that constraining all four parameters remains challenging: a_t is not constrained by any dataset, constraints on w_m and $\Delta_{\rm de}$ remain weak, only w_0 is well constrained across all datasets. The results further show that $w_0 > -1$, while w_m is negative, indicating a phantom-like behavior at early times. Interestingly, despite its larger parameter space, the proposed model shows a preference over the ΛCDM and w_0w_aCDM scenarios for certain combined datasets, according to both $\Delta\chi^2$ and Bayesian evidence, although this preference is not strong.

Unified Astronomy Thesaurus concepts: Cosmology (343); Dark energy (351); Cosmological parameters (339); Hubble constant (758); Cosmological models (337)

1. Introduction

The late-time accelerating expansion of our Universe, A. G. Riess et al. (1998), S. Perlmutter et al. (1999) was a groundbreaking discovery that opened new avenues in cosmology and astrophysics. This observation clearly indicated that a cosmological model based solely on ordinary matter cannot explain the observed acceleration. Instead, it requires the presence of a hypothetical component with sufficiently negative pressure, commonly referred to as dark energy (DE). However, the true nature, origin, and evolution of this mysterious component remain elusive. The simplest and most widely studied candidate for DE is a positive cosmological constant Λ, corresponding to the vacuum energy within the framework of Einstein's General Relativity (GR). When included in the gravitational field equations of GR, Λ alone can account for the accelerating expansion. It is characterized by a barotropic equation of state $w_\Lambda = p_\Lambda/\rho_\Lambda = -1$, where ρ_Λ and p_Λ are the energy density and pressure of the vacuum, respectively.[6] Current cosmological observations suggest that Λ contributes roughly 68% of the total energy budget of the Universe. The remaining 32% is dominated by cold (pressureless) dark matter (CDM), accounting for about 28%. This concordance model, composed of Λ and CDM, is known as the ΛCDM model. It has become the standard cosmological paradigm due to its success in fitting a wide range of independent observations. Nonetheless, it is well known that the ΛCDM model faces several unresolved challenges, such as the cosmological constant problem (S. Weinberg 1989), the cosmic coincidence problem (I. Zlatev et al. 1999), and a series of persistent cosmological tensions (E. Di Valentino et al. 2021, 2025; E. Abdalla et al. 2022; L. Perivolaropoulos & F. Skara 2022). These issues suggest that ΛCDM may be an incomplete description of the Universe's evolution. As a result, numerous efforts have been made to extend or revise the standard model, either by introducing time-dependent dark energy within GR, modifying gravity, or proposing entirely new frameworks. Many such models have been proposed to better capture the Universe's expansion history (see, for example, the reviews (P. J. E. Peebles & B. Ratra 2003; E. J. Copeland et al. 2006; S. Nojiri & S. D. Odintsov 2006; V. Sahni & A. Starobinsky 2006; A. De Felice & S. Tsujikawa 2010; T. P. Sotiriou & V. Faraoni 2010; K. Bamba et al. 2012; T. Clifton et al. 2012; Y.-F. Cai et al. 2016; K. Koyama 2016; S. Bahamonde et al. 2023 and references therein). However, none of these alternatives has yet emerged as a definitive model capable of explaining all current observations and resolving the existing anomalies. This motivates the search for new cosmological models that can better address the shortcomings of ΛCDM and reconcile the discrepancies in current astronomical data.

One of the simplest yet compelling extensions of the ΛCDM model involves modifying the DE sector through its barotropic equation of state (EoS), $w_{\rm de} = p_{\rm de}/\rho_{\rm de}$, where $p_{\rm de}$ and $\rho_{\rm de}$ are the pressure and energy density of DE, respectively. This EoS can be either constant—departing from $w = -1$, or time dependent. A constant EoS with $w_{\rm de} \neq -1$ gives rise to the

[6] As $\Lambda > 0$, vacuum energy density is positive, which implies a negative pressure and thus drives acceleration.

well-known wCDM cosmological model, in which DE is confined to either the quintessence regime ($w_{\rm de} > -1$) or the phantom regime ($w_{\rm de} < -1$), but disallows any crossing of the cosmological constant boundary, $w_{\rm de} = -1$. By contrast, time-dependent formulations of $w_{\rm de}$ are more flexible and allow for richer phenomenology. These models are particularly intriguing in light of recent observations from DESI, which do not rule out a dynamical DE EoS (A. G. Adame et al. 2025; M. Abdul Karim et al. 2025). DESI's analysis, based on the widely used Chevallier–Polarski–Linder (CPL) parameterization ($w_{\rm de}(a) = w_0 + w_a(1-a)$) (M. Chevallier & D. Polarski 2001; E. V. Linder 2003), suggests that models with evolving EoS remain viable (A. G. Adame et al. 2025; M. Abdul Karim et al. 2025). Similar conclusions were also reported in other recent analyses considering different DE parametrizations (W. Giarè et al. 2025; W. J. Wolf et al. 2025). Although the choice of $w_{\rm de}(a)$ is often phenomenological due to the lack of a guiding theoretical principle, this freedom has led to a wide range of models with varying numbers of free parameters: from zero-parameter forms to highly flexible multiparameter scenarios (A. R. Cooray & D. Huterer 1999; G. Efstathiou 1999; M. Chevallier & D. Polarski 2001; B. A. Bassett et al. 2003; P. S. Corasaniti & E. J. Copeland 2003; E. V. Linder 2003; U. Alam et al. 2004; P. S. Corasaniti et al. 2004; M. Kunz et al. 2004; C. Wetterich 2004; Y.-g. Gong & Y.-Z. Zhang 2005; H. K. Jassal et al. 2005; E. V. Linder & D. Huterer 2005; B. Feng et al. 2006; A. Melchiorri et al. 2006; E. M. Barboza & J. S. Alcaniz 2008; J.-F. Zhang et al. 2008; J.-Z. Ma & X. Zhang 2011; A. De Felice et al. 2012; C.-J. Feng et al. 2012; H. Li & X. Zhang 2012; I. Sendra & R. Lazkoz 2012; B. Novosyadlyj et al. 2014; O. Akarsu et al. 2015; N. Dimakis et al. 2016; M. Rezaei et al. 2017, 2024, 2025; D. Wang & X.-H. Meng 2017; S. Pan et al. 2018, 2020a, 2020b; W. Yang et al. 2018, 2019a, 2019b; 2021a, 2021b; X. Li & A. Shafieloo 2019; M. Rezaei 2019, 2024; H. B. Benaoum et al. 2022; R. K. Sharma et al. 2022; T.-Y. Yao et al. 2022; R. von Marttens et al. 2023; M. Cortês & A. R. Liddle 2024; B. R. Dinda 2024; R. Fikri et al. 2025; I. D. Gialamas et al. 2025; W. Giarè 2025a; W. Giarè et al. 2024, 2025; A. Hernández-Almada et al. 2024; J.-Q. Jiang et al. 2024; A. Lewis & E. Chamberlain 2025; J.-X. Li & S. Wang 2025; T.-N. Li et al. 2025a, 2025b; O. Luongo & M. Muccino 2024; N. Menci et al. 2024; M. Najafi et al. 2024; L. Orchard & V. H. Cárdenas 2024; S. Pourojaghi et al. 2025; O. F. Ramadan et al. 2024; M. Reyhani et al. 2024; S. Roy Choudhury & T. Okumura 2024; D. Shlivko & P. J. Steinhardt 2024; Y. Tada & T. Terada 2024; H. Wang & Y.-S. Piao 2026; W. Yin 2024; J. Zheng et al. 2025; A. Notari et al. 2024a, 2024b; C.-G. Park et al. 2024, 2025; Y. Carloni et al. 2025; E. Chaussidon et al. 2025; H. Cheng et al. 2025a, 2025b; G.-H. Du et al. 2025; L. A. Escamilla et al. 2025; Q. Gao et al. 2025; A. Gómez-Valent & J. Solà Peracaula 2025; A. González-Fuentes & A. Gómez-Valent 2025; L. Herold & T. Karwal 2025; M. Ishak & L. Medina-Varela 2025; D. A. Kessler et al. 2025; D. H. Lee et al. 2025; T. Liu et al. 2025; K. Lodha et al. 2025a; G. S. Nair et al. 2025; A. Paliathanasis 2025; A. Paliathanasis et al. 2025; Y.-H. Pang et al. 2025; J.a. Rebouças et al. 2025; S. Roy Choudhury 2025; M. A. Sabogal & R. C. Nunes 2025; E. Özülker et al. 2025; F. B. M. dos Santos et al. 2025; M. Scherer et al. 2025; A. J. Shajib & J. A. Frieman 2025; E. Silva & R. C. Nunes 2025; J.-Y. Song et al. 2025; E. Specogna et al. 2025; E. M. Teixeira et al. 2025; W. J. Wolf et al. 2025; G. Ye et al. 2025; Q. Zhou & S. Zheng 2025). Despite this proliferation, no single parameterization has emerged as strongly preferred by the data. In this context, any $w_{\rm de}$ model that remains consistent with observations continues to be worth investigating, especially as upcoming high-precision surveys may help distinguish among them or reveal subtle signatures of dark energy evolution.

Given the absence of theoretical guidance on the optimal number of free parameters in a $w_{\rm de}$ model, and the limited exploration in the literature of DE parametrizations with more than two parameters, in this article we investigate a four-parameter $w_{\rm de}$ model originally proposed in P. S. Corasaniti & E. J. Copeland (2003). The novelty of this parameterization lies in its ability to simultaneously capture key aspects of DE dynamics: the EoS at both early and late times, the scale factor at which the transition between these regimes occurs, and the sharpness of this transition. To the best of our knowledge, this model has seldom been studied in the context of DE cosmology. One likely reason is its relatively high computational cost due to the increased number of free parameters, which may lead to degeneracies and weaker constraints. However, with the rapid improvement in the precision of cosmological observations and the availability of extensive datasets spanning a wide redshift range, a reexamination of such a flexible model is timely and potentially insightful for uncovering subtle features of DE.

The structure of the paper is as follows. In Section 2, we introduce the dynamical dark energy (DDE) model under consideration. Section 3 describes the observational datasets used to constrain the model. In Section 4, we present and analyze the results. Finally, Section 5 provides a summary and concluding remarks.

2. Model

We consider the spatially flat Friedmann–Lemaître–Robertson–Walker (FLRW) line element of our Universe, which approximates it on large scales. This line element is given by $ds^2 = -dt^2 + a^2(t)(dx^2 + dy^2 + dz^2)$, in which $a(t)$ refers to the expansion scale factor of the Universe in terms of the cosmic time t, and (t, x, y, z) are the comoving coordinates. Assuming GR in the background, the Hubble equation can be written as $H^2 = (\kappa^2/3) \times (\rho_{\rm b} + \rho_{\rm r} + \rho_\nu + \rho_{\rm c} + \rho_{\rm de})$, in which κ^2 is Einstein's gravitational constant and ρ_i is the energy density of the ith component (b stands for baryons, r stands for radiation, ν stands for neutrinos, c and de correspond to CDM and DE, respectively). Under the assumption of no interaction between the fluids, one can determine the evolution of each individual component separately.[7] In what follows, we focus on the evolution of the dark energy sector, whose equation of state is given by (P. S. Corasaniti & E. J. Copeland 2003; P. S. Corasaniti et al. 2004):

$$w_{\rm de}(a) = w_0 + (w_m - w_0)\mathcal{G}(a), \tag{1}$$

[7] Let us note that, as commonly adopted in the literature, in this article, the sum of the neutrino masses is fixed to 0.06 eV and the number of neutrino species is fixed to $N_{\rm eff} = 3.044$.

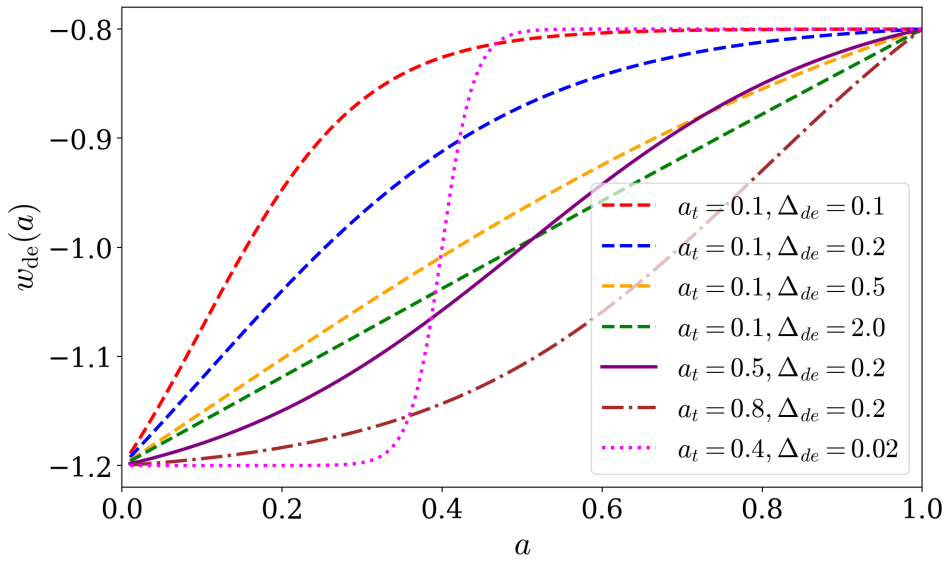

Figure 1. Evolution of $w_{\rm de}(a)$ for different sets of values of $a_{\rm t}$ and $\Delta_{\rm de}$, with the parameters w_0 and $w_{\rm m}$ fixed to -0.8 and -1.2, respectively.

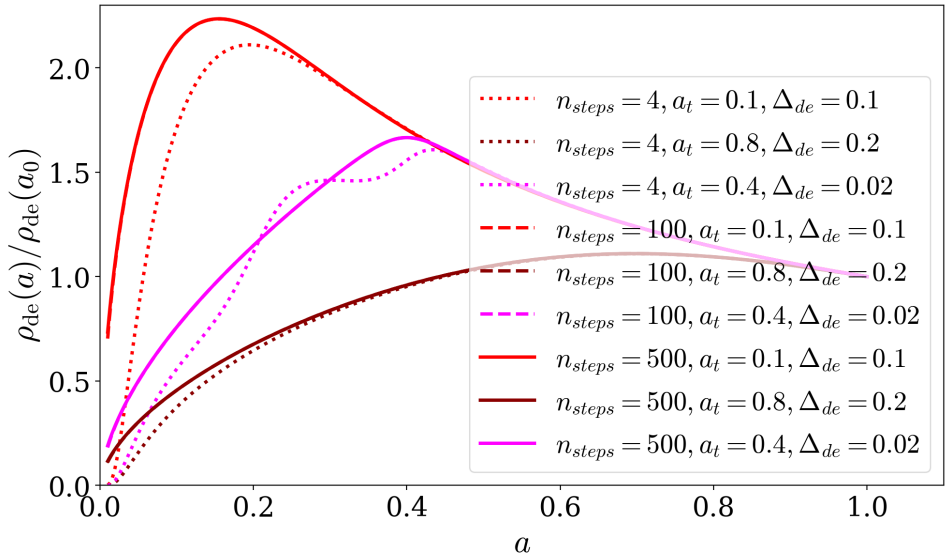

Figure 2. Evolution of $\frac{\rho_{\rm de}(a)}{\rho_{\rm de}(a_0)}$ for different sets of values for $n_{\rm steps}$, $a_{\rm t}$, and $\Delta_{\rm de}$, where the integral steps are set to $n_{\rm steps} = 4$, 100, and 500, respectively. The parameters w_0 and $w_{\rm m}$ are fixed to -0.8 and -1.2, respectively. Note that the curves for $n_{\rm steps} = 100$ and $n_{\rm steps} = 500$ overlap, demonstrating that the integral converges sufficiently at $n_{\rm steps} = 100$.

where $\mathcal{G}(a)$ is given by

$$\mathcal{G}(a) = \frac{1 - \exp(-(a-1)/\Delta_{\rm de})}{1 - \exp(1/\Delta_{\rm de})} \times \frac{1 + \exp(a_t/\Delta_{\rm de})}{1 + \exp(-(a-a_t)/\Delta_{\rm de})}. \quad (2)$$

In the above description of the DE EoS, w_0 refers to the present-day value of the DE EoS, w_m is the initial value of $w_{\rm de}$, i.e., $w_{\rm de} = w_m (a \ll 1)$, a_t corresponds to the scale factor at which the transition from w_m to w_0 occurs, and $\Delta_{\rm de}$ denotes the steepness of the transition. Therefore, Equation (1) contains four free parameters that need to be constrained. For the above EoS of DE, the energy density of the DE sector can be found from the following integral:

$$\rho_{\rm de} = \rho_{\rm de,0}\, a^{-3} \times \exp\left(-3 \int_{a_0=1}^{a} \frac{w_{\rm de}(a')}{a'}\, da'\right). \quad (3)$$

Now, considering the evolution of DE and other fluids present in the Hubble equation, one can, in principle, determine the expansion history of the Universe at the background level. Figures 1 and 2 provide a clear evolutionary history of the DE EoS, $w_{\rm de}(a)$, and its energy density in terms of $\rho_{\rm de}/\rho_{\rm de,0}$, considering different values of a_t and $\Delta_{\rm de}$. We note that while computing the integral in (3), we have used different integral steps $n_{\rm steps}$ in order to check the robustness achieved for a specific $n_{\rm steps}$. After comparing three different cases for $n_{\rm steps} = 4$, $n_{\rm steps} = 100$, and $n_{\rm steps} = 500$, we find that the

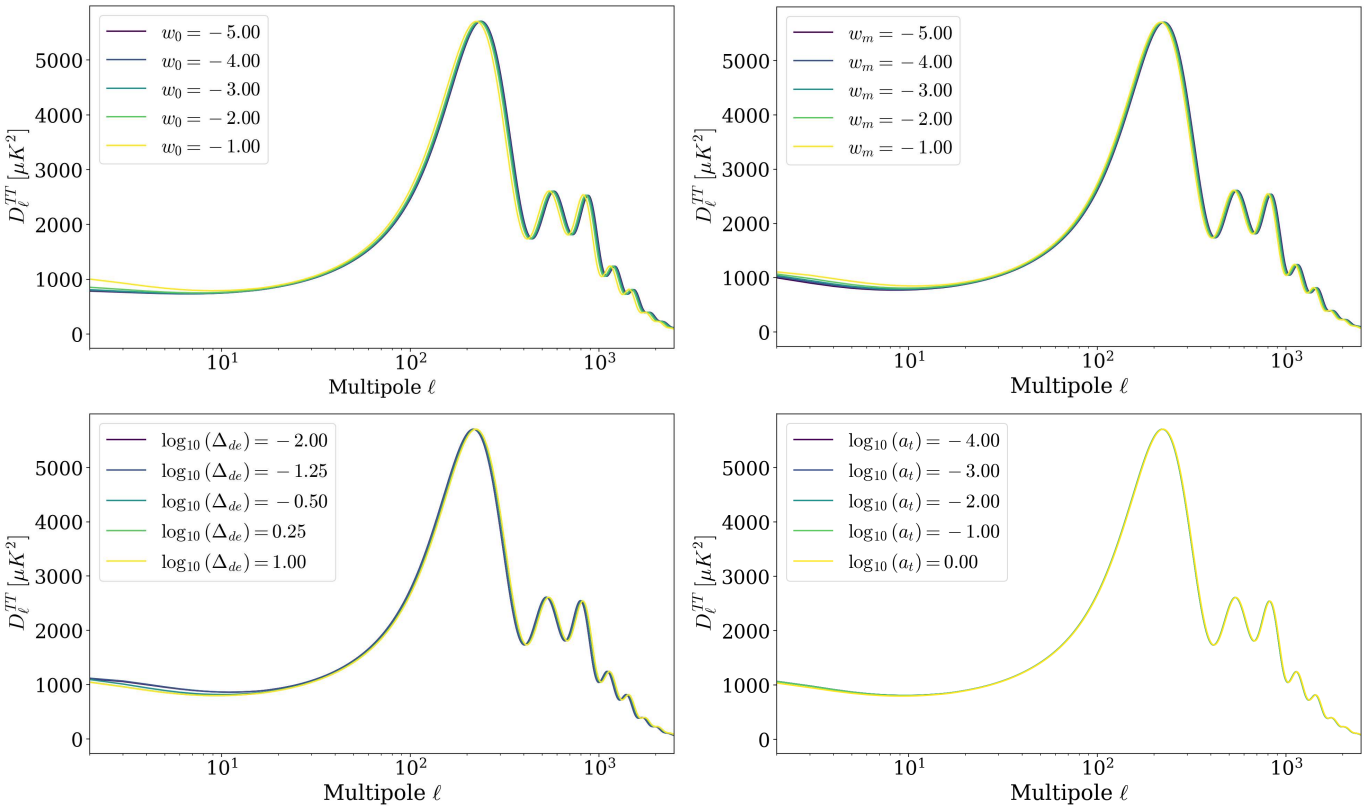

Figure 3. Theoretical prediction demonstrating the impact on the CMB TT power spectrum when varying different dark energy equation-of-state parameters (see the legends), while keeping the other EoS parameters fixed to the values $w_0 = -0.8$, $w_m = -2.2$, $\log_{10}(\Delta_{de})=-0.2$, and $\log_{10}(a_t)=-1$. Other cosmological parameters are fixed to the Planck 2018 best-fit values.

evolution of $\rho_{de}(a)$ for $n_{steps} = 100$ is indistinguishable from that obtained for $n_{steps} = 500$ (see Figure 2). This perfect overlap indicates that numerical convergence is reached; therefore, the integral of $\rho_{de}(a)$ is robust for $n_{steps} = 100$.[8]

We now turn our attention to the behavior of the model at the perturbative level. Following (C.-P. Ma & E. Bertschinger 1995), the evolution of all components at the perturbative level can be derived straightforwardly. Choosing the synchronous gauge, the perturbed version of the spatially flat FLRW metric in terms of the conformal time τ reads (C.-P. Ma & E. Bertschinger 1995) $ds^2 = a^2(\tau)[-d\tau^2 + (\delta_{ij} + h_{ij})dx^i dx^j]$. Taking into account the perturbed gravitational equations, one can then obtain the evolution equations for the individual fluids appearing in the Hubble equation (see also W. Giarè et al. (2024, 2025)). In the above metric, δ_{ij} denotes the unperturbed spatial part of the metric tensor, while h_{ij} represents the perturbed spatial part. In terms of the dimensionless density perturbation of the ith fluid, $\delta_i \equiv \delta\rho_i/\rho_i$, and the divergence of its velocity field, $\theta_i \equiv ik^j v_j$, in Fourier space, the evolution equations take the form

$$\delta_i' = -(1+w_i)\left(\theta_i + \frac{h'}{2}\right) - 3\mathcal{H}\left(\frac{\delta P_i}{\delta\rho_i} - w_i\right) \times \delta_i - 9\mathcal{H}^2\left(\frac{\delta P_i}{\delta\rho_i} - c_{a,i}^2\right)(1+w_i)\frac{\theta_i}{k^2}, \quad (4)$$

$$\theta_i' = -\mathcal{H}\left(1 - 3\frac{\delta P_i}{\delta\rho_i}\right)\theta_i + \frac{\delta P_i/\delta\rho_i}{1+w_i}\,k^2\,\delta_i - k^2\sigma_i, \quad (5)$$

where the prime denotes differentiation with respect to conformal time, $' \equiv d/d\tau$, $\mathcal{H}(a)$ is the conformal Hubble parameter, and h is the usual synchronous-gauge metric perturbation. Here, k denotes the wavenumber in Fourier space. The quantity σ_i represents the anisotropic stress of the ith fluid; in this work, we set $\sigma_i = 0$. Furthermore, $\delta P_i/\delta\rho_i$ defines the square of the sound speed of the i-th fluid in its rest frame. In particular, $\delta P_{de}/\delta\rho_{de} \equiv c_{s,de}^2$ corresponds to the sound speed of the dark energy component. The adiabatic sound speed is given by $c_{a,i}^2 = w_i - w_i'/[3\mathcal{H}(1+w_i)]$. Following the existing literature, we set $c_{s,de}^2 = 1$, as appropriate for minimally coupled scalar field models, and $c_{s,c}^2 = 0$.

Finally, in Figure 3, we show the impact on the cosmic microwave background (CMB) TT power spectrum when a particular DE parameter is varied while other parameters are fixed. We have shown four different plots where the four parameters of the DE EoS are individually varied. While drawing the plots, the other cosmological parameters are fixed to the Planck 2018 best-fit values using Planck 2018 TT,TE, EE+lowE+lensing (N. Aghanim et al. 2020a). In the upper left plot of Figure 3, we show the effects on the CMB TT spectrum for varying w_0 while fixing the other free parameters ($w_m = -2.2$, $\log_{10}(\Delta_{de})=-0.2$, $\log_{10}(a_t)=-1$). From this plot, one can see that changes in the low multipole region appear for different values of w_0. In particular, going deeply phantom leads to a suppression of the late-time ISW plateau. The upper

[8] Considering the robustness, during the statistical analysis, we set $n_{steps} = 100$ inside CAMB A. Lewis et al. (2000).

right panel of Figure 3 shows the impact on the CMB TT power spectrum for different values of w_m, keeping the remaining free parameters fixed ($w_0 = -0.8$, $\log_{10}(\Delta_{de})=-0.2$, $\log_{10}(a_t)=-1$). From this plot, one can see that there is no suppression of the ISW plateau, but we do observe a shift of the high-multipole peaks toward larger ℓ as w_m becomes very negative, although less pronounced than in the w_0 case. A similar effect is found in the lower left plot of Figure 3, where we varied Δ_{de} in terms of its logarithmic value, keeping the other parameters fixed ($w_0 = -0.8$, $w_m = -2.2$, $\log_{10}(a_t)=-1$). As $\log_{10}(\Delta_{de})$ increases from negative to positive values, the same shift in the high-ℓ peaks is observed. This suggests a negative correlation between Δ_{de} and w_m in their effect on the spectrum. In the lower right panel of Figure 3, we illustrate the impact of the transition scale factor a_t on the CMB TT power spectrum by varying $\log_{10}(a_t)$ while keeping the other dark energy parameters fixed ($w_0 = -0.8$, $w_m = -2.2$, $\log_{10}(\Delta_{de})=-0.2$). We find that variations in a_t do not produce any noticeable changes in the CMB TT spectrum, neither at low multipoles nor at high multipoles, even when the magnitude of $\log_{10}(a_t)$ is significantly increased. This behavior reflects the fact that a_t primarily controls the timing of the dark energy transition, which occurs at late times when dark energy affects the CMB only through the late Integrated Sachs–Wolfe effect. For the range of values explored, the resulting evolution of the gravitational potentials remains nearly unchanged, leading to a negligible impact on the CMB anisotropies. Consequently, a_t remains largely unconstrained by current CMB data.

3. Observational Data and Statistical Methodology

To perform parameter inference, we utilize the `Cobaya` tool (J. Torrado & A. Lewis 2021), which implements a Markov Chain Monte Carlo (MCMC) sampler specifically designed for cosmological analyses. This is coupled with an adapted version of the `CAMB` Boltzmann solver (A. Lewis et al. 2000), modified to incorporate our Dynamic Dark Energy (DDE) parameterization. Perturbations in DE are modeled using the standard parameterized post-Friedmann (PPF) approach provided in `CAMB` A. Lewis et al. (2000). The convergence of the MCMC chains is assessed by evaluating the Gelman-Rubin statistic $R-1$ A. Gelman & D. Rubin (1992), with convergence accepted at $R-1<0.02$. Posterior distributions and parameter contours are analyzed and visualized via the `getdist` package (A. Lewis 2025).

For a comprehensive comparison of the four-parameter DE models, we use the following observational datasets:

1. *CMB*. Cosmic Microwave Background (CMB) measurements from the Planck 2018 legacy data release, incorporating high-ℓ Plik TT, TE, and EE likelihoods, the low-ℓ TT-only Commander likelihood, and the low-ℓ EE-only SimAll likelihood (N. Aghanim et al. 2020b, 2020c, 2020d), combined with the Planck 2018 lensing likelihood (N. Aghanim et al. 2020d). This integrated dataset is collectively referred to as CMB.
2. *BAO*. Baryon Acoustic Oscillation (BAO) measurements from the initial 3 yr of the Dark Energy Spectroscopic Instrument (DESI DR2) (M. Abdul Karim et al. 2025, U. Andrade et al. 2025, K. Lodha et al. 2025b) labeled as DESI.

Table 1
Flat Prior Distributions Imposed on the Cosmological Parameters Used in Our Analysis

Model	Parameter	Prior
ΛCDM	$\Omega_b h^2$	[0.005, 0.1]
ΛCDM	$\Omega_c h^2$	[0.001, 0.99]
ΛCDM	τ	[0.01, 0.8]
ΛCDM	$100\,\theta_s$	[0.5, 10]
ΛCDM	$\ln(10^{10}A_s)$	[1.61, 3.91]
ΛCDM	n_s	[0.8, 1.2]
4PDE	w_0	[−5.0 , 0.0]
4PDE	w_m	[−5.0 , −0.5]
4PDE	$\log_{10}(\Delta_{de})$	[−3.0 , 1.0]
4PDE	$\log_{10}(a_t)$	[−4.0 , 0.0]

Note. The 4PDE models include the standard ΛCDM parameters along with four additional parameters.

3. *Type Ia Supernovae*. Distance modulus observations from Type Ia Supernovae (SNeIa) sourced from the PantheonPlus compilation (D. Brout et al. 2022, D. Scolnic et al. 2022), encompassing 1701 light curves from 1550 distinct SNeIa spanning the redshift range $z\in[0.001, 2.26]$, referred to as PantheonPlus. Additionally, we incorporate the full 5 yr dataset from the Dark Energy Survey (DES), comprising 1635 SNeIa across redshifts $0.1<z<1.13$ (T. M. C. Abbott et al. 2024, B. O. Sánchez et al. 2024, M. Vincenzi et al. 2024), referred to as DESY5, and the Union3 compilation, comprising 2087 SNe (D. Rubin et al. 2025) denoted as Union3.

We apply uniform flat priors as specified in Table 1. The expanded four-parameter DE models are structured as extensions of the standard six-parameter ΛCDM model. This baseline consists of the baryon density $\Omega_b h^2$, cold dark matter density $\Omega_c h^2$, reionization optical depth τ_{reio}, scalar amplitude and spectral index $\ln(10^{10}A_s)$ and n_s, and the angular size at recombination of the sound horizon θ_s. To this baseline, we append four additional dark energy equation-of-state parameters, detailed in Section 2.

To quantify the statistical performance of the extended four-parameter DE (4PDE) model relative to the standard ΛCDM model, we evaluate the differences in the minimum chi-square values. We note that the total χ^2 for each model is obtained by summing the contributions from the individual datasets (CMB, BAO, and SN). In statistical parlance, combining these likelihoods under the assumption of independence constitutes a composite likelihood approach (B. G. Lindsay et al. 2011, C. Varin et al 2011). While this method formally approximates the full joint distribution, it is well motivated in this context, given the distinct physical regimes probed and the negligible cross-correlations among the selected datasets. The difference is defined as:

$$\Delta\chi^2_{\mathrm{min},\Lambda\mathrm{CDM/CPL}} = \chi^2_{\mathrm{min,4PDE}} - \chi^2_{\mathrm{min},\Lambda\mathrm{CDM/CPL}}. \quad (6)$$

A negative value of the difference in Equation (6) indicates that the data favor the extended 4PDE model over the ΛCDM or CPL model. Furthermore, we perform Bayesian model comparison by computing the logarithm of the Bayesian evidence $\ln\mathcal{Z}$ using `MCEvidence` (A. Heavens et al. 2017),

Table 2
Observational Constraints at 68% CL and Upper or Lower Limits at 95% CL Using Various Datasets

Parameters	CMB +DESY5	CMB +PantheonPlus	CMB +Union3	CMB +DESI	CMB+DESI +DESY5	CMB+DESI +PantheonPlus	CMB+DESI +Union3
$\Omega_b h^2$	0.02241 ± 0.00015	0.02240 ± 0.00015	0.02241 ± 0.00014	0.02241 ± 0.00014	0.02243 ± 0.00013	0.02245 ± 0.00014	0.02244 ± 0.00013
$\Omega_c h^2$	0.1196 ± 0.0012	0.1196 ± 0.0012	0.1195 ± 0.0012	0.11948 ± 0.00095	0.11915 ± 0.00091	0.11899 ± 0.00095	0.11920 ± 0.00090
$100\,\theta_{MC}$	1.04096 ± 0.00032	1.04097 ± 0.00031	1.04097 ± 0.00031	1.04099 ± 0.00029	1.04101 ± 0.00028	1.04106 ± 0.00028	1.04101 ± 0.00028
τ_{reio}	0.0526 ± 0.0076	$0.0533^{+0.0067}_{-0.0076}$	0.0524 ± 0.0072	0.0522 ± 0.0073	0.0537 ± 0.0071	0.0547 ± 0.0074	0.0534 ± 0.0071
n_s	0.9662 ± 0.0041	0.9663 ± 0.0041	0.9664 ± 0.0041	0.9667 ± 0.0037	0.9673 ± 0.0037	0.9678 ± 0.0037	0.9673 ± 0.0037
$\ln(10^{10} A_s)$	3.040 ± 0.015	3.041 ± 0.014	3.039 ± 0.014	3.039 ± 0.014	3.041 ± 0.014	3.043 ± 0.014	3.041 ± 0.014
w_0	$-0.820^{+0.099}_{-0.14}$	$-0.927^{+0.032}_{-0.083}$	$-0.74^{+0.15}_{-0.19}$	-0.57 ± 0.24	-0.804 ± 0.066	$-0.899^{+0.050}_{-0.062}$	-0.74 ± 0.10
w_m	$-2.39^{+1.3}_{-0.65}$	<-1.15	$-2.57^{+1.3}_{-0.73}$	$-2.41^{+0.92}_{-0.52}$	$-2.18^{+1.1}_{-0.44}$	$-2.58^{+1.6}_{-0.89}$	$-2.28^{+1.0}_{-0.35}$
$\log_{10}(\Delta_{de})$	…	…	…	>-1.03	>-0.896	-0.63 ± 0.70	$-0.15^{+0.49}_{-0.71}$
$\log_{10}(a_t)$	…	…	…	…	…	…	…
H_0 [km/s/Mpc]	67.0 ± 1.2	$67.50^{+0.94}_{-1.5}$	66.8 ± 1.5	$64.8^{+2.1}_{-2.4}$	66.94 ± 0.56	67.71 ± 0.59	66.27 ± 0.87
σ_8	0.807 ± 0.013	$0.811^{+0.011}_{-0.014}$	0.805 ± 0.015	$0.788^{+0.018}_{-0.020}$	0.8048 ± 0.0087	0.8105 ± 0.0091	0.799 ± 0.010
S_8	0.831 ± 0.012	0.829 ± 0.012	0.832 ± 0.012	0.839 ± 0.014	0.8279 ± 0.0094	0.8238 ± 0.0098	0.831 ± 0.010
Ω_m	0.319 ± 0.013	$0.314^{+0.014}_{-0.011}$	0.320 ± 0.015	0.341 ± 0.024	0.3175 ± 0.0056	0.3099 ± 0.0057	0.3242 ± 0.0088
$\Delta\chi^2_{min,\Lambda CDM}$	-6.95	-2.62	-4.83	-9.96	-18.54	-10.91	-13.58
$\Delta \ln \mathcal{Z}_{\Lambda CDM}$	-1.92	-4.75	-2.52	-1.25	2.57	-1.45	0.67
$\Delta\chi^2_{min,CPL}$	0.46	-0.33	0.23	0.47	0.19	-3.74	0.74
$\Delta \ln \mathcal{Z}_{CPL}$	-0.54	0.27	-0.65	-0.38	0.03	1.14	-0.24

Note. Here, $\Delta\chi^2_{min}$ and $\Delta \ln \mathcal{Z}$ are defined as $\Delta\chi^2_{min,\Lambda CDM/CPL} = \chi^2_{min,4PDE} - \chi^2_{min,\Lambda CDM/CPL}$ and $\Delta \ln \mathcal{Z}_{\Lambda CDM/CPL} \equiv \ln \mathcal{Z}_{4PDE} - \ln \mathcal{Z}_{\Lambda CDM/CPL}$. Negative values of $\Delta\chi^2_{min,\Lambda CDM/CPL}$ favor the 4PDE model over the standard ΛCDM/CPL scenario, while positive values of $\Delta \ln \mathcal{Z}_{\Lambda CDM/CPL}$ indicate a preference for the 4PDE model.

interfaced through the `Cobaya` wrapper available in the `wgcosmo` repository (W. Giare 2025b). According to Bayes' theorem, for each model $\mathcal{M}_i$ characterized by parameters Θ, the posterior distribution is:

$$P(\Theta|D, \mathcal{M}_i) = \frac{\mathcal{L}(D|\Theta, \mathcal{M}_i)\,\pi(\Theta|\mathcal{M}_i)}{\mathcal{Z}_i}, \tag{7}$$

where $\mathcal{L}$ denotes the maximum likelihood, π represents the prior, and the evidence $\mathcal{Z}_i$ is computed as:

$$\mathcal{Z}_i = \int \mathcal{L}(D|\Theta, \mathcal{M}_i)\,\pi(\Theta|\mathcal{M}_i)\,\mathrm{d}\Theta. \tag{8}$$

For model comparison, we calculate the Bayes factor $\mathcal{Z}_{\Lambda\mathrm{CDM/CPL}} = \mathcal{Z}_{\mathrm{4PDE}}/\mathcal{Z}_{\Lambda\mathrm{CDM/CPL}}$, and define the relative log-evidence as:

$$\Delta \ln \mathcal{Z}_{\Lambda\mathrm{CDM/CPL}} \equiv \ln \mathcal{Z}_{\mathrm{4PDE}} - \ln \mathcal{Z}_{\Lambda\mathrm{CDM/CPL}}, \tag{9}$$

Positive values of $\Delta \ln \mathcal{Z}_{\Lambda\mathrm{CDM/CPL}}$ indicate support for the extended model.

We interpret $\Delta \ln \mathcal{Z}_{\Lambda\mathrm{CDM/CPL}}$ using the updated Jeffreys' scale (R. E. Kass & A. E. Raftery 1995): ranges of [0, 1] imply *inconclusive* evidence, [1, 2.5] suggest *weak* evidence, [2.5, 5] denote *moderate* evidence, [5, 10] reflect *strong* evidence, and values exceeding 10 represent *very strong* evidence supporting the favored model.

4. Results and Their Implications

This section is devoted to the observational constraints of the 4PDE model. To this end, we use the latest cosmological probes, namely CMB, BAO, and three different compilations of SNeIa (DESY5, PantheonPlus, and Union3), and perform various combined analyses. Additionally, we compare the present model with respect to the ΛCDM model in terms of $\Delta\chi^2_{\mathrm{min},\Lambda\mathrm{CDM}}$ and $\Delta \ln \mathcal{Z}_{\Lambda\mathrm{CDM}}$. In Table 2, we present the constraints on the free and derived parameters of this model, and in Figures 4, 5, 6, and 7 we graphically illustrate its behavior. As the number of free parameters in this model is significantly larger than in common DE parameterizations, the constraining power of CMB data alone is limited. Therefore, instead of performing a CMB-only analysis, we initially consider two combinations: CMB+SNeIa and CMB+DESI. We then perform a full analysis using the combined dataset CMB+DESI+SNeIa to improve parameter constraints. In the following, we discuss the results obtained from each combined dataset.

We begin with the first three analyses: CMB+DESY5, CMB +PantheonPlus, and CMB+Union3. Examining the results on the free and derived parameters, our first observation is that the parameter w_0, which represents the present-day value of the DE EoS, lies in the quintessence regime at slightly more than 68% CL for both CMB+DESY5 and CMB+Union3. In the case of CMB +PantheonPlus, although the mean value of w_0 also falls in the quintessence regime, it remains consistent with a cosmological constant $w_0 = -1$ within the 68% CL ($w_0 = -0.927^{+0.032}_{-0.083}$). The parameter w_m, denoting the initial value of the DE EoS, shows a phantom behavior at more than 68% CL in the CMB+DESY5 and CMB+Union3 combinations ($w_m = -2.39^{+1.3}_{-0.65}$ and $w_m = -2.57^{+1.3}_{-0.73}$, respectively). For CMB+PantheonPlus, however, w_m is only weakly constrained, with an upper limit $w_m < -1.15$ at 95% CL. The possibility of phantom DE at early times is also supported by recent DESI results (R. Calderon et al. 2024, K. Lodha et al. 2025b). On the other hand, the parameters a_t (the scale factor at which the transition from w_m to w_0 occurs) and Δ_{de} (the steepness of the transition) remain unconstrained by these datasets, as also illustrated in Figure 4. The derived parameters H_0, S_8, and Ω_m from all three combined datasets closely match the values reported by Planck under the ΛCDM assumption (N. Aghanim et al. 2020a), albeit with slightly larger uncertainties due to the increased number of free parameters in the model. Regarding model comparison, we find that the 4PDE model is statistically favored over ΛCDM in terms of the minimum chi-square values, with $\Delta\chi^2_{\mathrm{min},\Lambda\mathrm{CDM}} < 0$ for all three combinations—most notably for CMB+DESY5, but also for CMB+PantheonPlus and CMB+Union3. However, the Bayesian evidence penalizes the model due to its higher complexity, and as a result, ΛCDM is preferred for all three datasets. This preference is strongest for the CMB+PantheonPlus combination, with $\Delta \ln \mathcal{Z}_{\Lambda\mathrm{CDM}}=-4.75$, compared to $\Delta \ln \mathcal{Z}_{\Lambda\mathrm{CDM}} = -1.92$ for CMB+DESY5 and $\Delta \ln \mathcal{Z}_{\Lambda\mathrm{CDM}}=-2.52$ for CMB+Union3.

We now consider the dataset CMB+DESI and its combinations with three distinct SNeIa compilations (see also Figure 5): CMB+DESI+DESY5, CMB+DESI+PantheonPlus, and CMB+DESI+Union3. For CMB+DESI alone, we observe that the mean value of w_0 is significantly shifted away from -1 ($w_0 = -0.57 \pm 0.24$ at 68% CL), and it remains in the quintessence regime at approximately 1.8σ. The DE EoS at early times remains in the phantom regime, quantified by the parameter w_m, which takes the value $w_m = -2.41^{+0.92}_{-0.52}$ at 68% CL, consistent with a phantom behavior at more than 1σ. Regarding the other two free parameters, we find that a_t remains unconstrained, similar to what we observed in the earlier CMB+SNeIa analyses, while Δ_{de} receives a lower bound: $\log_{10}(\Delta_{\mathrm{de}}) > -1.03$ at 95% CL. It is worth noting that recent DESI results (R. Calderon et al. 2024, E. Özülker et al. 2025, K. Lodha et al. 2025b) indicate a preference for phantom crossing around $a \sim 0.7$. However, in our case, since the steepness of the transition (Δ_{de}) is treated as a free parameter, this flexibility broadens the posterior distribution of a_t, rendering it unconstrained. Turning to the derived parameters, we find that CMB+DESI yields a relatively low value of the Hubble constant, $H_0 = 64.8^{+2.1}_{-2.4}$ km s^{-1} Mpc^{-1} at 68% CL, compared to the Planck baseline result assuming ΛCDM N. Aghanim et al. (2020a). This notably low value of H_0 is driven by the behavior of w_0. The CMB+DESI combination pushes w_0 significantly away from -1, and, due to the well-known geometric degeneracy between w_0 and H_0, which arises from the fact that the CMB tightly constrains the angular diameter distance to the last scattering surface, this shift in w_0 translates into a lower inferred value of H_0 (see Figure 5). Consequently, owing to the geometric degeneracy between H_0 and the matter density parameter Ω_m, which originates from the fact that the CMB primarily constrains the combination $\Omega_m h^2$ ($=\Omega_c h^2 + \Omega_b h^2$) rather than Ω_m and H_0 separately, Ω_m assumes a higher value than the Planck baseline, with $\Omega_m = 0.341 \pm 0.024$ at 68% CL. From the model comparison perspective, the χ^2 analysis shows that CMB+DESI favors the 4PDE model over ΛCDM, with $\Delta\chi^2_{\mathrm{min},\Lambda\mathrm{CDM}}=-9.96$. However, the Bayesian evidence penalizes the extra model complexity, and the comparison instead favors ΛCDM, albeit weakly, according to the revised Jeffreys' scale ($\Delta \ln \mathcal{Z}_{\Lambda\mathrm{CDM}}=-1.25$).

Now, when DESY5 is combined with CMB+DESI (i.e., for the combined dataset CMB+DESI+DESY5), we find that the

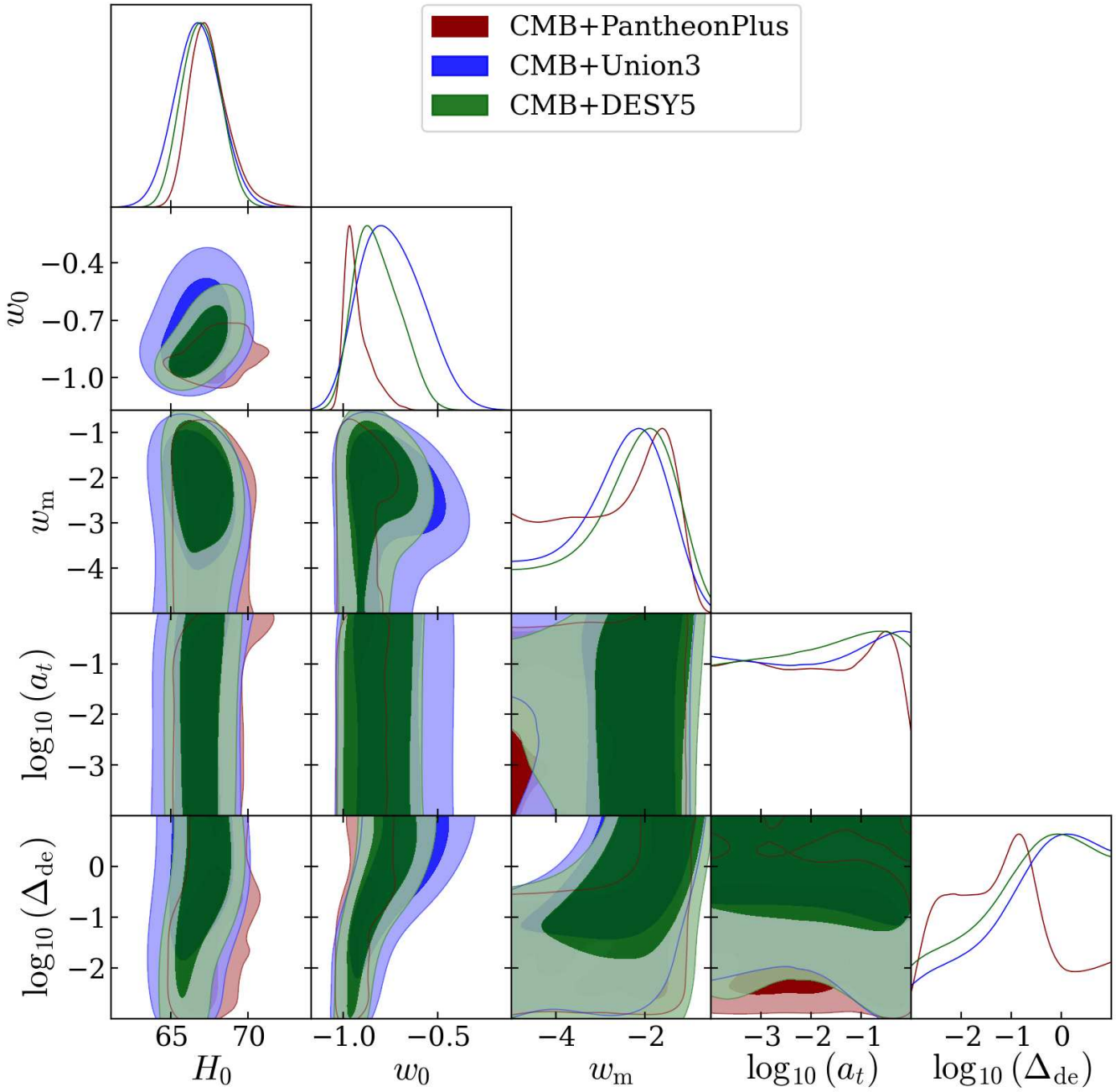

Figure 4. One-dimensional posterior distributions and two-dimensional marginalized contours for H_0 and the four model parameters, as obtained from the CMB +PantheonPlus, CMB+Union3, and CMB+DESY5 dataset combinations.

mean value of w_0 shifts closer to -1 ($w_0 = -0.804 \pm 0.066$ at 68% CL), while its deviation from the cosmological constant increases to approximately 2.97σ, strengthening its quintessence-like nature. The parameter w_m remains in the phantom regime at roughly 1σ significance. Among the remaining two parameters, $\Delta_{\rm de}$ receives a lower bound ($\log_{10}\Delta_{\rm de} > -0.896$ at 95% CL), but a_t continues to remain unconstrained. The derived parameters H_0 and S_8 are consistent with the Planck baseline values under ΛCDM (N. Aghanim et al. 2020a). Notably, the inclusion of DESY5 with CMB+DESI significantly reduces the uncertainties in the parameter space compared to the CMB+DESI case alone. A particularly interesting result in this case is that both the χ^2 analysis and the Bayesian evidence support the 4PDE model over ΛCDM. In particular, we find a substantial improvement in the fit: $\Delta\chi^2_{\rm min,\Lambda CDM} = -18.54$, with a positive Bayes factor of $\Delta \ln \mathcal{Z}_{\Lambda\rm CDM} = 2.57$, indicating moderate evidence in favor of the 4PDE model. In Figure 6, a graphical comparison between $\Delta\chi^2_{\rm min,\Lambda CDM}$ and $\Delta \ln \mathcal{Z}_{\Lambda\rm CDM}$ clearly illustrates the preference for the 4PDE model in the CMB+DESI+DESY5 dataset. A mild preference is also observed for the CMB+DESI+Union3 combination, which will be discussed in the following paragraph.

The next two combined datasets, CMB+DESI+PantheonPlus and CMB+DESI+Union3, are particularly interesting because, among all dataset combinations explored in this work,

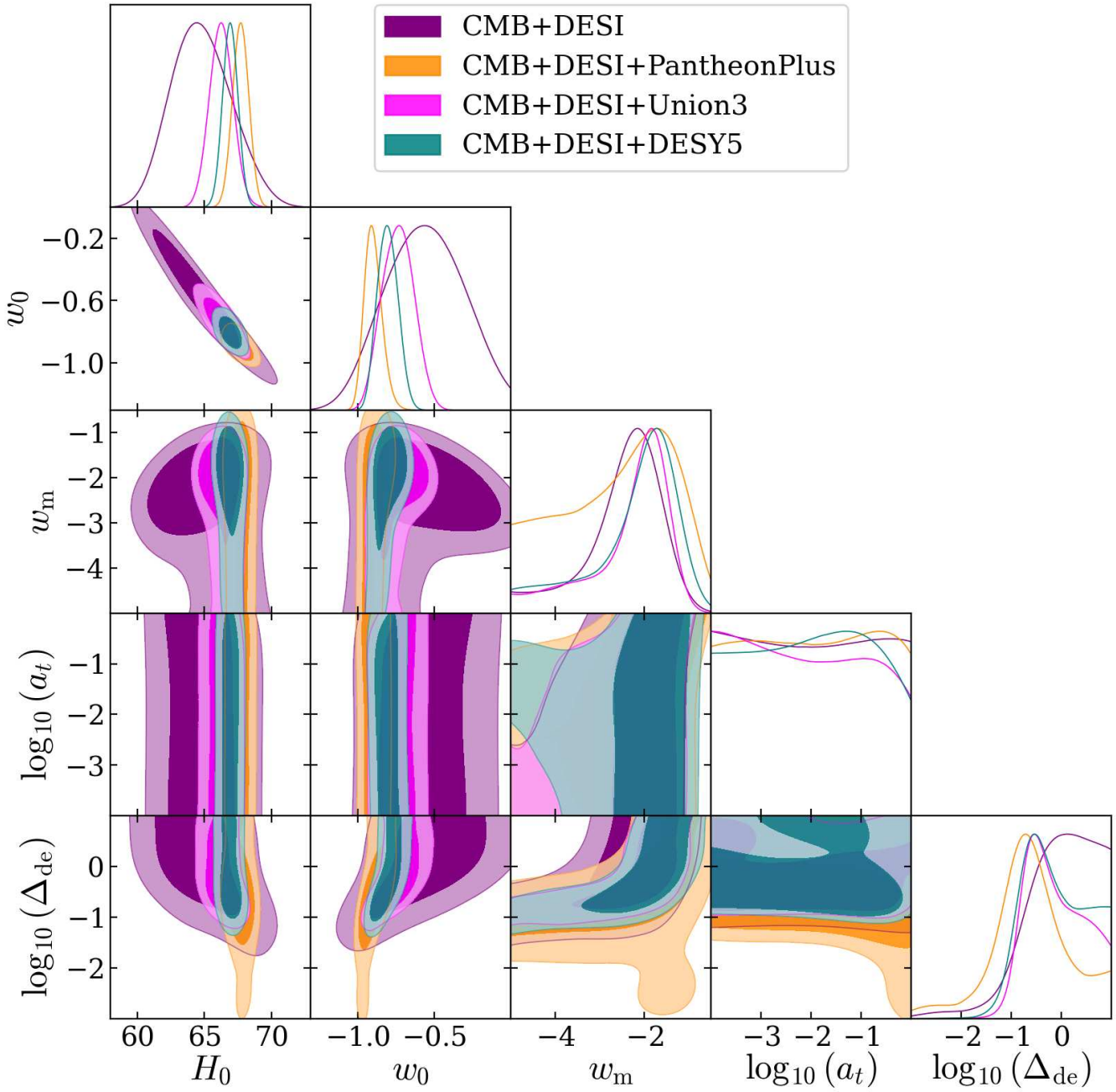

Figure 5. One-dimensional posterior distributions and two-dimensional marginalized contours for H_0 and the four model parameters, as obtained from the CMB +DESI, CMB+DESI+PantheonPlus, CMB+DESI+Union3, and CMB+DESI+DESY5 dataset combinations.

these are the only cases where $\Delta_{\rm de}$ becomes constrained. Specifically, we find $\log_{10}\Delta_{\rm de} = -0.63 \pm 0.70$ (68% CL, CMB+DESI+PantheonPlus) and $\log_{10}\Delta_{\rm de} = -0.15^{+0.49}_{-0.71}$ (68% CL, CMB+DESI+Union3). However, in both cases, the parameter a_t remains unconstrained. The present-day value of the DE equation of state, w_0, is pushed closer to -1 compared to CMB+DESI alone ($w_0 = -0.57 \pm 0.24$ at 68% CL). In particular, we obtain $w_0 = -0.899^{+0.050}_{-0.062}$ (CMB+DESI +PantheonPlus) and $w_0 = -0.74 \pm 0.10$ (CMB+DESI +Union3), both at 68% CL. This places w_0 firmly in the quintessence regime ($w > -1$), corresponding to a deviation from the phantom divide ($w_{\rm de} = -1$) at approximately 2σ for CMB+DESI+PantheonPlus and 2.6σ for CMB+DESI +Union3. The early-time EoS parameter w_m retains a phantom-like behavior, with its statistical significance varying across the datasets. The derived parameters, such as H_0 and Ω_m, show only minor deviations from Planck (under ΛCDM) (N. Aghanim et al. 2020a). For CMB+DESI +Union3, we find $H_0 = 66.27 \pm 0.87$ km s^{-1} Mpc^{-1} and $\Omega_m = 0.3242 \pm 0.0088$ at 68% CL, indicating a mild shift. In contrast, the values returned by CMB+DESI+PantheonPlus are fully consistent with those of Planck within ΛCDM. Finally, regarding model comparison statistics, the χ^2 analysis shows a preference for the 4PDE model over ΛCDM in both combinations ($\Delta\chi^2_{\rm min,\Lambda CDM} < 0$). However, the Bayesian evidence provides a more nuanced picture: only CMB

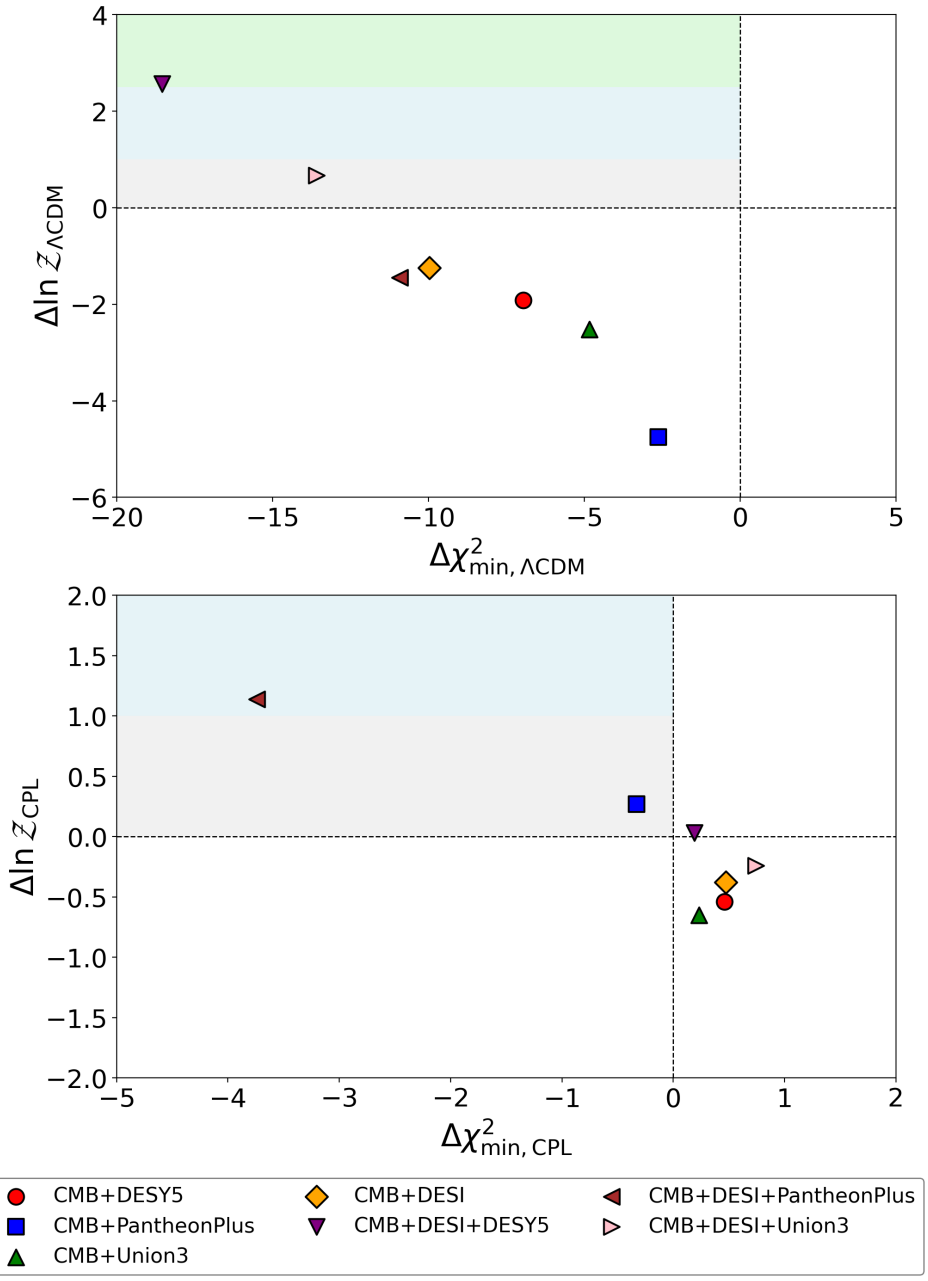

Figure 6. $\Delta\chi^2_{\mathrm{min},\Lambda\mathrm{CDM}}$ *versus* $\Delta \ln \mathcal{Z}_{\Lambda\mathrm{CDM}}$ and $\Delta\chi^2_{\mathrm{min,CPL}}$ versus $\Delta \ln \mathcal{Z}_{\mathrm{CPL}}$ for the 4PDE model, considering all datasets.

+DESI+Union3 very mildly favors the 4PDE model, with $\Delta \ln \mathcal{Z}_{\Lambda\mathrm{CDM}} = 0.67$, which is classified as *inconclusive* under the revised Jeffreys' scale. On the other hand, CMB+DESI +PantheonPlus shows a preference for ΛCDM, with $\Delta \ln \mathcal{Z}_{\Lambda\mathrm{CDM}} = -1.45$. Taken together, these results present a mixed picture in terms of model preference, depending on the dataset combination and statistical criterion employed.

Before concluding this section, we investigate additional cosmological quantities that provide further insight into the behavior of the 4PDE model. In Figure 7, we show the evolution of the normalized dark energy density, $\rho_{\mathrm{de}}(a)/\rho_{\mathrm{de}}(a_0)$ (left panel), and the dark energy equation of state $w_{\mathrm{de}}(a)$ (right panel), using MCMC samples from the CMB+DESI, CMB+DESI+DESY5, and CMB+DESI +PantheonPlus datasets. The evolution of $\rho_{\mathrm{de}}(a)$ reveals an emergent behavior: it grows from early times, reaches a maximum, and then begins to decline. However, we note that this reconstructed evolution is comparable to that allowed by the CPL parameterization. Therefore, in terms of reconstructing the dark energy evolution history, the present 4PDE analysis does not reveal any distinctive features beyond those already captured by standard two-parameter models. In contrast, the equation of state $w_{\mathrm{de}}(a)$ shows a transition from a phantom regime in the past to a quintessence regime at late times, crossing the phantom divide line, as also seen in recent analyses (H. Cheng et al. 2025a; E. Özülker et al. 2025). This phantom-to-quintessence transition is reminiscent of the behavior found in the CPL parameterization, particularly in DESI analyses (M. Abdul Karim et al. 2025). Similar features have been observed in other two-parameter models of dark energy, as discussed in W. Giarè et al. (2024), suggesting that the dynamical behavior captured by our four-parameter model

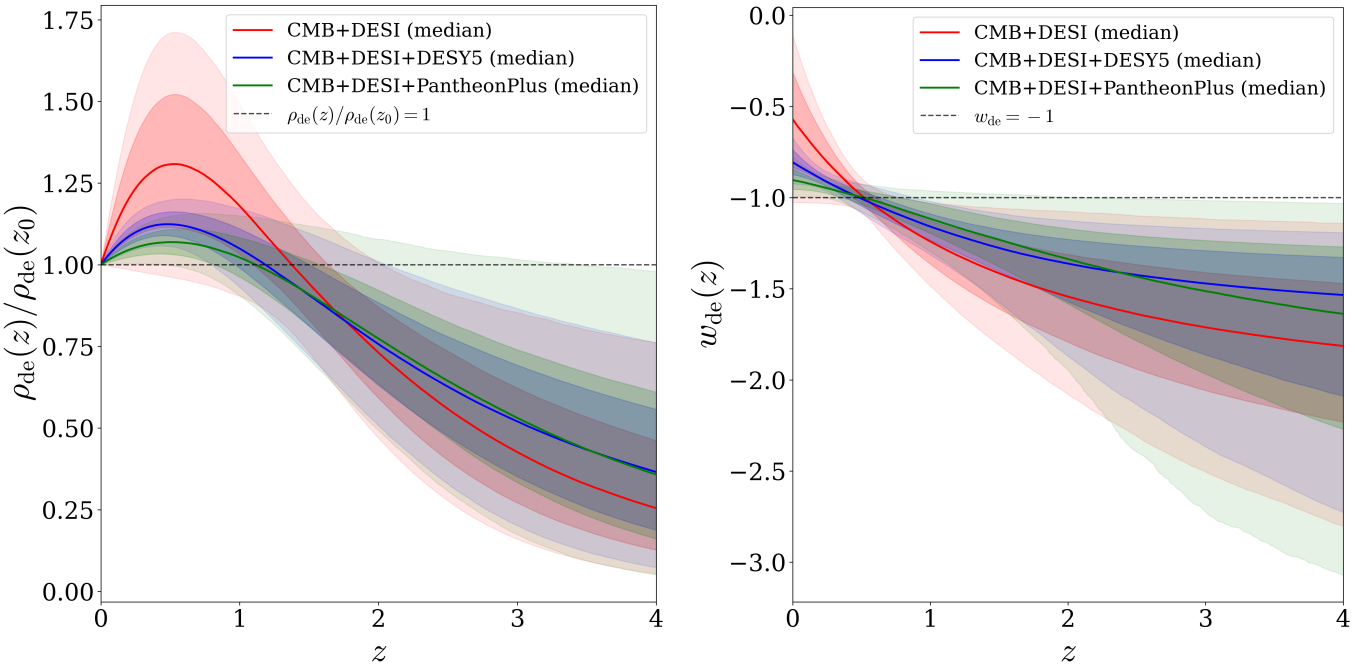

Figure 7. Evolution of the normalized DE density $\rho_{de}(z)/\rho_{de}(z_0)$ (left panel) and the DE EoS $w_{de}(z)$ (right panel) as functions of the redshift z, based on MCMC samples using the combined datasets CMB+DESI, CMB+DESI+DESY5, and CMB+DESI+PantheonPlus, where $\rho_{de}(z_0)$ is the DE density at the present day ($z = 0$).

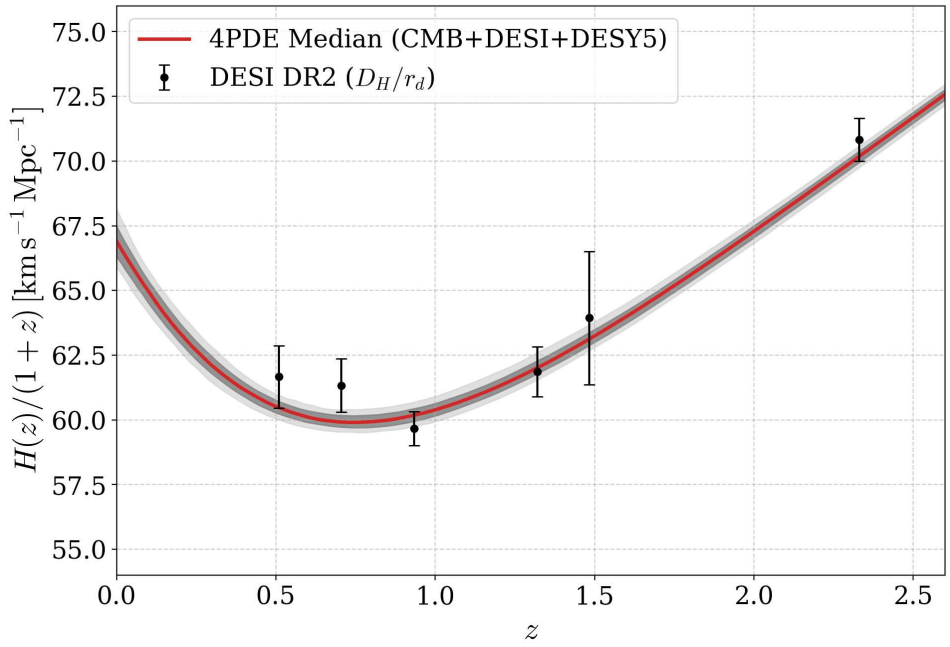

Figure 8. Comoving Hubble parameter, shown as $H(z)/(1 + z)$, as a function of redshift z. The black data points with error bars are from DESI DR2, derived from the ratio of the Hubble distance to the sound horizon, D_H/r_d. The solid red line indicates the median curve, and the gray bands show the 68% and 95% confidence ranges allowed by CMB+DESI+DESY5 in the 4PDE model.

aligns well with recent trends in observational cosmology. In Figure 8, we present the best-fit evolution of the comoving Hubble parameter $H(z)/(1 + z)$, including 1σ and 2σ confidence bands, for the 4PDE model. These results are compared against the DESI DR2 data for D_H/r_d. We focus on the CMB+DESI+DESY5 combination, which offers the strongest statistical support for the 4PDE model among the datasets considered. As shown in the figure, the 4PDE model provides an excellent match to the DESI data, especially at high redshift. Finally, in Figure 9, we compare the predictions of the 4PDE model and ΛCDM for three different BAO distance measurements from DESI, again using the CMB +DESI+DESY5 dataset. The bottom panel of Figure 9 shows the normalized residuals between theoretical predictions and observational data: circles represent ΛCDM, and crosses correspond to the 4PDE model. As evident from the residuals,

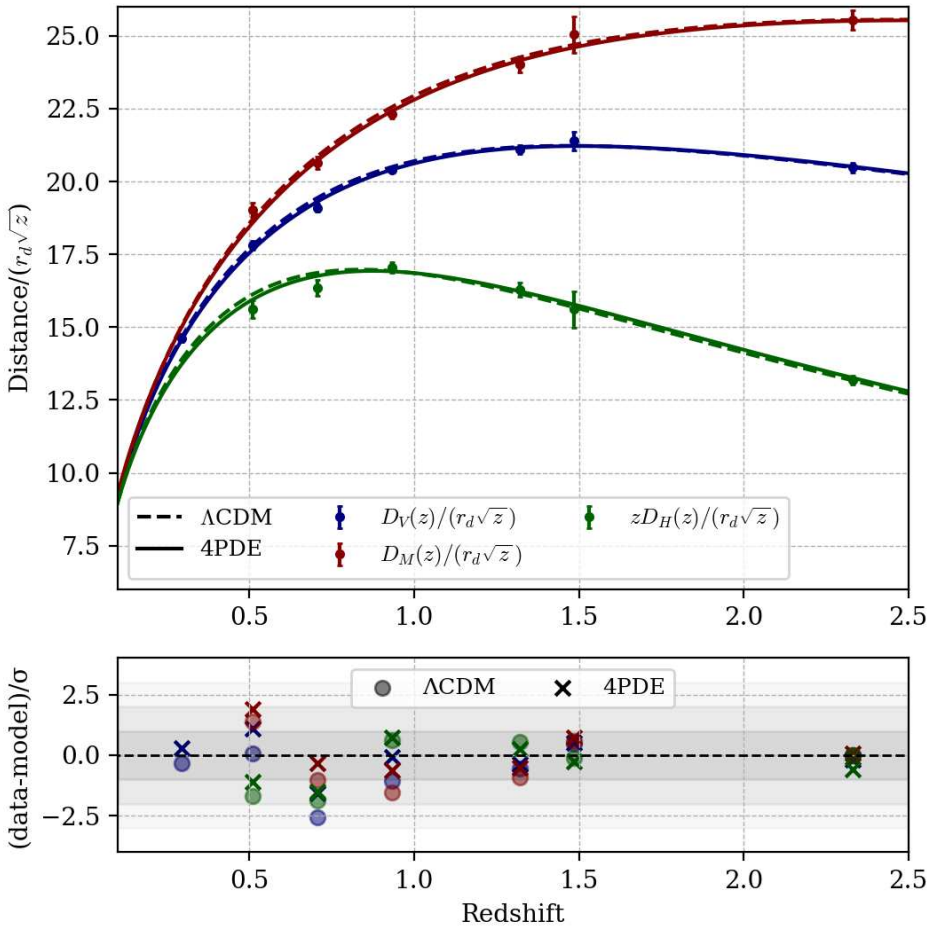

Figure 9. Top panel: BAO distance measurements. The solid lines represent the best-fit 4PDE model, while the dashed lines depict the best-fit standard ΛCDM model. Both models are constrained using the CMB+DESI+DESY5 dataset combination. Bottom panel: the residuals for each model, showing the difference between the data and the model predictions, normalized by the measurement uncertainty σ. Circles correspond to the ΛCDM model, and crosses correspond to the 4PDE model.

the 4PDE model is generally favored across most redshift bins, consistent with the trend observed in Figure 6, where this dataset combination shows the strongest preference for the 4PDE scenario.

5. Summary and Conclusions

This article investigates a four-parameter dynamical dark energy (4PDE) model aimed at understanding the evolution of dark energy from early times to the present. The free parameters of the model are: w_0 (the present-day value of the dark energy equation of state, EoS), w_m (its early-time value), a_t (the scale factor at which the transition from w_m to w_0 occurs), and $\Delta_{\rm de}$ (the steepness of the transition). This parameterization was originally introduced by Corasaniti and Copeland (P. S. Corasaniti & E. J. Copeland 2003), and more recently revisited in R. K. Sharma et al. (2022). However, unlike other widely studied dynamical dark energy (DDE) models, this and similar four-parameter extensions have not received much attention in the literature. A likely reason is the large number of free parameters, which can lead to degeneracies and weaker constraints. Nonetheless, two important considerations motivate renewed attention to such models. First, the true nature of dark energy remains unknown, and a range of observational studies, both model-dependent and nonparametric, support the possibility of dynamical behavior. While the CPL parameterization remains a popular benchmark, the broader search for alternative DDE models is ongoing. Second, the sensitivity and redshift coverage of cosmological datasets are rapidly improving, and previously unconstrained or degenerate parameters may become distinguishable with new data.

In this work, we constrain the 4PDE model using the latest cosmological datasets, including CMB (Planck 2018), BAO from DESI DR2, and three supernova compilations: Pantheon-Plus, DESY5, and Union3. The results are summarized in Table 2, with graphical representations provided in Figures 4, 5, 6, 7, 8, and 9. We find that constraining all four parameters remains challenging: a_t is not constrained by any dataset, while the constraints on w_m and $\Delta_{\rm de}$ remain weak. Only the present-day value of the dark energy equation of state, w_0, is well constrained across all datasets. This indicates that current cosmological probes do not yet have the sensitivity required to simultaneously constrain the full dynamics of this four-parameter extension. Our results consistently indicate a quintessential nature for dark energy at present, with a phantom-like behavior in the past.

One of the key outcomes of this analysis is that, despite the increased number of free parameters compared to ΛCDM, the 4PDE model is statistically favored according to both $\Delta\chi^2$ and

Bayesian evidence for the CMB+DESI+DESY5 combination, which shows moderate evidence in its favor.[9] In contrast, the analysis yields inconclusive evidence for the CMB+DESI +Union3 combination. For the remaining dataset combinations, the standard ΛCDM model remains preferred. In addition to the comparison with ΛCDM, we assess the statistical performance of the 4PDE model against the CPL parameterization in Table 2. For the majority of dataset combinations, the two models are statistically indistinguishable. The differences in both the goodness of fit and the Bayesian evidence are negligible, with $|\Delta\chi^2_{\rm min,CPL}| < 1$ and $|\Delta \ln \mathcal{Z}_{\rm CPL}| < 1$. Although the 4PDE model occupies a significantly larger prior volume due to its additional free parameters, it does not incur the expected Bayesian penalty. This indicates that the extra parameters, in particular $\log_{10}(a_t)$ and $\log_{10}(\Delta_{\rm de})$, remain largely unconstrained by these datasets. When the data are unable to significantly reduce the allowed parameter space, the posterior volume remains comparable to the prior volume ($V_{\rm posterior} \approx V_{\rm prior}$), effectively canceling the Occam's razor penalty typically associated with increased model complexity. A notable exception is the CMB+DESI +PantheonPlus combination, which favors the 4PDE model with an improvement of $\Delta\chi^2_{\rm min,CPL} = -3.74$, and a positive evidence gain of $\Delta \ln \mathcal{Z}_{\rm CPL} = 1.14$. This preference arises because this specific dataset combination provides tighter constraints on $\log_{10}(\Delta_{\rm de})$, allowing the model to effectively exploit its extended parameter freedom to achieve a better fit to the data. In conclusion, while one dataset combination (CMB +DESI+PantheonPlus) hints at a weak preference for the 4PDE scenario, current observational data are generally insufficient to distinguish it from the simpler CPL model. This suggests that higher-precision data will be required to justify the inclusion of additional degrees of freedom in the dark energy sector. These findings suggest that four-parameter DDE models deserve further exploration, particularly with upcoming high-precision cosmological observations. Although one parameter (a_t) remains unconstrained in the current analysis, it remains to be investigated whether this is due to limitations of current data or inherent features of the model itself. The preference for this extended model in some dataset combinations provides a compelling motivation to revisit richer DDE parameterizations in future work.

Acknowledgments

We thank the referee for many insightful comments, which resulted in an improved version of the manuscript. H.C. acknowledges the support of the China Scholarship Council (CSC) program (Project ID No. 202406230341). H.C. also acknowledges the support by the National Natural Science Foundation of China (NSFC) through the grant No. 12350610240 "Astrophysical Axion Laboratories." S.P. acknowledges the partial support by the Department of Science and Technology (DST), Govt. of India under the Scheme "Fund for Improvement of S&T Infrastructure (FIST)" (File No. SR/FST/MS-I/2019/41). E.D.V. is supported by a Royal Society Dorothy Hodgkin Research Fellowship. The authors acknowledge the use of High-Performance Computing resources from the IT Services at the University of Sheffield. This article is based on work from COST Action CA21136 Addressing observational tensions in cosmology with systematics and fundamental physics (CosmoVerse) supported by COST (European Cooperation in Science and Technology).

[9] The gain in evidence in favor of the 4PDE model due to DESY5 is not surprising, as the last two DESI data releases have shown that evidence for dynamical dark energy is more pronounced in the presence of DESY5 than for the other two SNeIa datasets (A. G. Adame et al. 2025, M. Abdul Karim et al. 2025). Although DESI also reported evidence for dynamical dark energy (assuming the CPL parameterization) when using the remaining two SNeIa datasets, however one cannot disregard the fact that such evidence depends on the underlying dark energy model as well.

ORCID iDs

Hanyu Cheng https://orcid.org/0000-0002-7445-6110
Supriya Pan https://orcid.org/0000-0001-9500-401X
Eleonora Di Valentino https://orcid.org/0000-0001-8408-6961

References

Abbott, T. M. C., et al. 2024, ApJL, 973, L14
Abdalla, E., et al. 2022, JHEAp, 34, 49
Abdul Karim, M., et al. 2025, PhRvD, 112, 083515
Adame, A. G., et al. 2025, JCAP, 02, 021
Aghanim, N., et al. 2020a, A&A, 641, 67
Aghanim, N., et al. 2020b, A&A, 641, 56
Aghanim, N., et al. 2020c, A&A, 641, 92
Aghanim, N., et al. 2020d, A&A, 641, 42
Akarsu, O., Dereli, T., & Vazquez, J. A. 2015, JCAP, 06, 049
Alam, U., Sahni, V., & Starobinsky, A. A. 2004, JCAP, 06, 008
Andrade, U., et al. 2025, PhRvD, 112, 083512
Bahamonde, S., Dialektopoulos, K. F., Escamilla-Rivera, C., et al. 2023, RPPh, 86, 026901
Bamba, K., Capozziello, S., Nojiri, S., & Odintsov, S. D. 2012, Ap&SS, 342, 155
Barboza, E. M., Jr., & Alcaniz, J. S. 2008, PhLB, 666, 415
Bassett, B. A., Kunz, M., Parkinson, D., & Ungarelli, C. 2003, PhRvD, 68, 043504
Benaoum, H. B., Yang, W., Pan, S., & Di Valentino, E. 2022, IJMPD, 31, 2250015
Brout, D., et al. 2022, ApJ, 938, 110
Cai, Y.-F., Capozziello, S., De Laurentis, M., & Saridakis, E. N. 2016, RPPh, 79, 106901
Calderon, R., et al. 2024, JCAP, 10, 048
Carloni, Y., Luongo, O., & Muccino, M. 2025, PhRvD, 111, 023512
Chaussidon, E., et al. 2025, arXiv:2503.24343
Cheng, H., Di Valentino, E., Escamilla, L. A., Sen, A. A., & Visinelli, L. 2025a, JCAP, 09, 031
Cheng, H., Di Valentino, E., & Visinelli, L. 2025b, arXiv:2505.22066
Chevallier, M., & Polarski, D. 2001, IJMPD, 10, 213
Clifton, T., Ferreira, P. G., Padilla, A., & Skordis, C. 2012, PhR, 513, 1
Cooray, A. R., & Huterer, D. 1999, ApJL, 513, L95
Copeland, E. J., Sami, M., & Tsujikawa, S. 2006, IJMPD, 15, 1753
Corasaniti, P. S., & Copeland, E. J. 2003, PhRvD, 67, 063521
Corasaniti, P. S., Kunz, M., Parkinson, D., Copeland, E. J., & Bassett, B. A. 2004, PhRvD, 70, 083006
Cortês, M., & Liddle, A. R. 2024, JCAP, 12, 007
De Felice, A., Nesseris, S., & Tsujikawa, S. 2012, JCAP, 05, 029
De Felice, A., & Tsujikawa, S. 2010, LRR, 13, 3
Dimakis, N., Karagiorgos, A., Zampeli, A., et al. 2016, PhRvD, 93, 123518
Dinda, B. R. 2024, JCAP, 09, 062
Di Valentino, E., Mena, O., Pan, S., et al. 2021, CQGra, 38, 153001
Di Valentino, E., et al. 2025, PDU, 49, 101965
dos Santos, F. B. M., Morais, J., Pan, S., Yang, W., & Di Valentino, E. 2025, arXiv:2504.04646
Du, G.-H., Wu, P.-J., Li, T.-N., & Zhang, X. 2025, EPJC, 85, 392
Efstathiou, G. 1999, MNRAS, 310, 842
Escamilla, L. A., Pan, S., Di Valentino, E., et al. 2025, PhRvD, 111, 023531
Feng, B., Li, M., Piao, Y.-S., & Zhang, X. 2006, PhLB, 634, 101
Feng, C.-J., Shen, X.-Y., Li, P., & Li, X.-Z. 2012, JCAP, 09, 023
Fikri, R., ElKhateeb, E., Lashin, E. S., & El Hanafy, W. 2025, AnPhy, 481, 170190
Gao, Q., Peng, Z., Gao, S., & Gong, Y. 2025, Univ, 11, 10
Gelman, A., & Rubin, D. 1992, StaSc, 7, 457

Gialamas, I. D., Hütsi, G., Kannike, K., et al. 2025, PhRvD, 111, 043540
Giarè, W. 2025a, PhRvD, 112, 023508
Giare, W. 2025b, wgcosmo: Cosmological Analysis Tools, GitHub. https://github.com/williamgiare/wgcosmo
Giarè, W., Mahassen, T., Di Valentino, E., & Pan, S. 2025, PDU, 48, 21
Giarè, W., Najafi, M., Pan, S., Di Valentino, E., & Firouzjaee, J. T. 2024, JCAP, 10, 035
Gómez-Valent, A., & Solà Peracaula, J. 2025, PhRvD, 864, 139391
Gong, Y.-g., & Zhang, Y.-Z. 2005, PhRvD, 72, 043518
González-Fuentes, A., & Gómez-Valent, A. 2025, JCAP, 12, 049
Heavens, A., Fantaye, Y., Mootoovaloo, A., et al. 2017, arXiv:1704.03472
Hernández-Almada, A., Mendoza-Martínez, M. L., García-Aspeitia, M. A., & Motta, V. 2024, PDU, 46, 10
Herold, L., & Karwal, T. 2025, arXiv:2506.12004
Ishak, M., & Medina-Varela, L. 2025, arXiv:2507.22856
Jassal, H. K., Bagla, J. S., & Padmanabhan, T. 2005, PhRvD, 72, 103503
Jiang, J.-Q., Pedrotti, D., da Costa, S. S., & Vagnozzi, S. 2024, PhRvD, 110 (12) 123519
Kass, R. E., & Raftery, A. E. 1995, JASA, 90, 773
Kessler, D. A., Escamilla, L. A., Pan, S., & Di Valentino, E. 2025, arXiv:2504.00776
Koyama, K. 2016, RPPh, 79, 046902
Kunz, M., Corasaniti, P.-S., Parkinson, D., & Copeland, E. J. 2004, PhRvD, 70, 041301
Lee, D. H., Yang, W., Di Valentino, E., Pan, S., & van de Bruck, C. 2025, arXiv:2507.11432
Lewis, A. 2025, JCAP, 08, 025
Lewis, A., Challinor, A., & Lasenby, A. 2000, ApJ, 538, 473
Lewis, A., & Chamberlain, E. 2025, JCAP, 05, 065
Li, H., & Zhang, X. 2012, PhLB, 713, 160
Li, J.-X., & Wang, S. 2025, JCAP, 07, 047
Li, T.-N., Du, G.-H., Zhou, S.-H., et al. 2025a, arXiv:2511.22512
Li, T.-N., Li, Y.-H., Du, G.-H., et al. 2025b, EPJC, 85, 608
Li, X., & Shafieloo, A. 2019, ApJL, 883, L3
Linder, E. V. 2003, PhRvL, 90, 091301
Linder, E. V., & Huterer, D. 2005, PhRvD, 72, 043509
Lindsay, B. G., Yi, G. Y., & Sun, J. 2011, Statistica Sinica, 21, 71–105 https://www.jstor.org/stable/24309263
Liu, T., Li, X., & Wang, J. 2025, ApJ, 988, 243
Lodha, K., et al. 2025a, PhRvD, 111, 023532
Lodha, K., et al. 2025b, arXiv:2503.14743
Luongo, O., & Muccino, M. 2024, A&A, 690, A40
Ma, C.-P., & Bertschinger, E. 1995, ApJ, 455, 7
Ma, J.-Z., & Zhang, X. 2011, PhLB, 699, 233
Melchiorri, A., Paciello, B., Serra, P., & Slosar, A. 2006, NJPh, 8, 325
Menci, N., Sen, A. A., & Castellano, M. 2024, ApJ, 976, 227
Nair, G. S., Chakraborty, A., Amendola, L., & Das, S. 2025, arXiv:2512.08752
Najafi, M., Pan, S., Di Valentino, E., & Firouzjaee, J. T. 2024, Phys. Dark Univ., 45, 14
Nojiri, S., & Odintsov, S. D. 2006, eConf, C0602061, 06
Notari, A., Redi, M., & Tesi, A. 2024a, JCAP, 11, 025
Notari, A., Redi, M., & Tesi, A. 2024b, arXiv:2411.11685
Novosyadlyj, B., Sergijenko, O., Durrer, R., & Pelykh, V. 2014, JCAP, 05, 030
Orchard, L., & Cárdenas, V. H. 2024, PDU, 46, 101678
Özülker, E., Di Valentino, E., & Giarè, W. 2025, arXiv:2506.19053
Paliathanasis, A. 2025, PDU, 48, 101956
Paliathanasis, A., Mengoni, T., Leon, G., & Luongo, O. 2025, arXiv:2512.00558
Pan, S., Saridakis, E. N., & Yang, W. 2018, PhRvD, 98, 063510
Pan, S., Yang, W., Di Valentino, E., Shafieloo, A., & Chakraborty, S. 2020a, JCAP, 06, 062
Pan, S., Yang, W., & Paliathanasis, A. 2020b, EPJC, 80, 274
Pang, Y.-H., Zhang, X., & Huang, Q.-G. 2025, arXiv:2503.21600
Park, C.-G., de Cruz Perez, J., & Ratra, B. 2025, IJMPD, 34, 2550058
Park, C.-G., Pérez, de C., & Ratra, J. 2024, PhRvD, 110, 13
Peebles, P. J. E., & Ratra, B. 2003, RvMP, 75, 559
Perivolaropoulos, L., & Skara, F. 2022, NewAR, 95, 106
Perlmutter, S., et al. 1999, ApJ, 517, 565
Pourojaghi, S., Malekjani, M., & Davari, Z. 2025, PhRvD, 111, 083547
Ramadan, O. F., Sakstein, J., & Rubin, D. 2024, PhRvD, 110, L041303
Rebouças, J.a., de Souza, D. H. F., Zhong, K., Miranda, V., & Rosenfeld, R. 2025, JCAP, 02, 024
Reyhani, M., Najafi, M., Firouzjaee, J. T., & Di Valentino, E. 2024, PDU, 44, 14
Rezaei, M. 2019, MNRAS, 485, 4841
Rezaei, M. 2024, ApJ, 967, 2
Rezaei, M., Malekjani, M., Basilakos, S., Mehrabi, A., & Mota, D. F. 2017, ApJ, 843, 65
Rezaei, M., Pan, S., Yang, W., & Mota, D. F. 2024, JCAP, 01, 052
Rezaei, M., Pan, S., Yang, W., & Mota, D. F. 2025, ApJ, 995, 164
Riess, A. G., et al. 1998, AJ, 116, 1009
Roy Choudhury, S. 2025, ApJL, 986, L31
Roy Choudhury, S., & Okumura, T. 2024, ApJL, 976, L11
Rubin, D., et al. 2025, ApJ, 986, 231
Sabogal, M. A., & Nunes, R. C. 2025, JCAP, 09, 084
Sahni, V., & Starobinsky, A. 2006, IJMPD, 15, 2105
Sánchez, B. O., et al. 2024, ApJ, 975, 5
Scherer, M., Sabogal, M. A., Nunes, R. C., & De Felice, A. 2025, PhRvD, 112, 043513
Scolnic, D., et al. 2022, ApJ, 938, 113
Sendra, I., & Lazkoz, R. 2012, MNRAS, 422, 776
Shajib, A. J., & Frieman, J. A. 2025, PhRvD, 112, 063508
Sharma, R. K., Pandey, K. L., & Das, S. 2022, ApJ, 934, 113
Shlivko, D., & Steinhardt, P. J. 2024, PhLB, 855, 138826
Silva, E., & Nunes, R. C. 2025, JCAP, 11, 078
Song, J.-Y., Du, G.-H., Li, T.-N., et al. 2025, arXiv:2511.12017
Sotiriou, T. P., & Faraoni, V. 2010, RvMP, 82, 451
Specogna, E., Adil, S. A., Ozulker, E., et al. 2025, arXiv:2504.17859
Tada, Y., & Terada, T. 2024, PhRvD, 109, L121305
Teixeira, E. M., Giarè, W., Hogg, N. B., et al. 2025, PhRvD, 112, 023515
Torrado, J., & Lewis, A. 2021, JCAP, 05, 057
Varin, C., Reid, N., & Firth, D. 2011, Statistica Sinica, 21, 5–42 https://www.jstor.org/stable/24309261
Vincenzi, M., et al. 2024, ApJ, 975, 86
von Marttens, R., Barbosa, D., & Alcaniz, J. 2023, JCAP, 04, 052
Wang, D., & Meng, X.-H. 2017, PhRvD, 96, 103516
Wang, H., & Piao, Y.-S. 2026, PhLB, 873, 140180
Weinberg, S. 1989, RvMP, 61, 1
Wetterich, C. 2004, PhLB, 594, 17
Wolf, W. J., García-García, C., & Ferreira, P. G. 2025, JCAP, 05, 034
Yang, W., Di Valentino, E., Pan, S., Shafieloo, A., & Li, X. 2021a, PhRvD, 104, 063521
Yang, W., Di Valentino, E., Pan, S., Wu, Y., & Lu, J. 2021b, MNRAS, 501, 5845
Yang, W., Pan, S., Di Valentino, E., & Saridakis, E. N. 2019a, Univ, 5, 219
Yang, W., Pan, S., Di Valentino, E., Saridakis, E. N., & Chakraborty, S. 2019b, PhRvD, 99, 043543
Yang, W., Pan, S., & Paliathanasis, A. 2018, MNRAS, 475, 2605
Yao, T.-Y., Guo, R.-Y., & Zhao, X.-Y. 2022, JHEP, 9, 1044
Ye, G., Martinelli, M., Hu, B., & Silvestri, A. 2025, PhRvL, 134, 181002
Yin, W. 2024, JHEP, 05, 327
Zhang, J.-F., Zhang, X., & Liu, H.-Y. 2008, MPLA, 23, 139
Zheng, J., Qiang, D.-C., & You, Z.-Q. 2025, JCAP, 08, 056
Zhou, Q., & Zheng, S. 2025, arXiv:2512.07104
Zlatev, I., Wang, L.-M., & Steinhardt, P. J. 1999, PhRvL, 82, 896